Tomislav Senčić
Tommaso Lucchini
Vedran Mrzljak

ISSN 1333-1124

TUNING AND VALIDATION OF A DIESEL SPRAY MODEL

UDC 621.436.038:519.61/.64:532.5

Summary

A spray model has been implemented in the OpenFOAM CFD toolkit. A set of constant volume chamber injection simulations has been performed in order to analyze the influence of the spray model constants. In the performed analysis, a set of model constants was selected and the simulation results were compared to the experimental results obtained in the Sandia constant volume combustion chamber.

The implemented model showed very good agreement with the experimental results with respect to the vapour penetration and spray shape. The simulated liquid penetration did not match the experimental results, but this is considered less important for combustion simulations.

Key words: *spray model, diesel injection, CFD simulation*

1. Introduction

Computer simulations are a very useful tool that helps us to develop modern direct injection diesel engines, to optimize their performance and to meet the latest restrictive emissions limits. CFD (Computational Fluid Dynamics) simulations [13] are the most complex level of mathematical models for engine simulation. However, they are necessary in some analyses if the geometry influence has to be evaluated. They are also necessary for the calculation of pollutant formation since the chemical reaction rates are highly influenced by the local temperature variations.

The fuel spray parameters have a great influence on the diesel engine performance and pollutant formation. The fuel liquid breakup (spray) determines the rate of evaporation, the fuel vapour distribution and the fuel-air mixture formation. These determine the combustion rate, the developed temperatures, and the chemical reaction rates and hence, pollutant formation. It means that it is very important to have an accurate numerical model for spray calculation in a CFD engine simulation.

Fuel spray breakup was investigated by various authors. The main spray parameters are the spray angle and penetration, Sauter mean diameter, and droplet size distribution. Hiroysu et al., [6], [7], provided some of the correlations used for these parameters. Heywood [5] also presents some of these correlations. Amsden et al., [1], [2], developed a computer program that allowed a further improvement of spray models. Reitz and al. analyzed the influence of the nozzle design and operating conditions on the fuel spray [11]. O'Rourke and al. proposed

a model based on an analogy between an oscillating and distorting droplet and a spring-mass system [12]. Reitz proposed a model based on the first order linear analysis of Kelvin-Helmholtz instability growing on the surface of a cylindrical liquid jet [10]. The Rayleigh-Taylor model (RT model) is based on the theoretical work of Taylor who investigated the instability of the interface between two fluids of different densities in the case of an acceleration (or deceleration) normal to this interface [3]. Kralj [8] analyzed the performances of the Huh and MPI models. Baumgarten collected and described different models that describe the processes from fuel injection to mixture formation [3].

OpenFOAM [14] is an open source, free CFD collection of solvers and libraries written in C++. Due to its availability, flexibility and the collaboration between users, it is a good platform to use to approach uncommon CFD problems such as diesel engine processes.

2. Spray model

Mathematical models are used to simulate fuel spray injection in internal combustion engines. There are different models available in the literature; some of them are mentioned in the introduction. Park and Lee [9] have validated the models against experimental data obtained for high-pressure diesel sprays under atmospheric conditions. The results concerning spray tip penetration and axial SMD distribution agree well with experimental data in the case of the KH-RT model.

Hence, in the current study, the KH-RT (Kelvin-Helmholtz - Rayleigh-Taylor) combination of models is used for spray breakup.

The Kelvin-Helmholtz (KH) model is based on the first order linear analysis of Kelvin-Helmholtz instability growing on the surface of a cylindrical liquid jet with the initial diameter 2 r_0 that is penetrating into a stationary incompressible gas with a relative velocity u_{rel}, Figure 1.

Due to the turbulence in the nozzle hole, the jet surface is covered with sinusoidal, axisymmetric surface waves. These surface waves grow because of aerodynamic forces due to the relative velocity between the liquid and gas.

The analysis of the problem described in detail in [10] yields an equation relating the growing rate ω (increase in the amplitude per unit time) of a perturbation to its wavelength $\lambda = 2\pi/k$:

$$\omega^2 + 2\nu_l k^2 \omega \left(\frac{I_1'(kr_0)}{I_0(kr_0)} - \frac{2kl}{k^2+l^2} \frac{I_1(kr_0)}{I_0(kr_0)} \frac{I_1'(lr_0)}{I_1(lr_0)} \right)$$
$$= \frac{\sigma k}{\rho_l r_0^2} \left(1 - r_0^2 k^2\right) \left(\frac{l^2 - k^2}{l^2 + k^2} \right) \frac{I_1(kr_0)}{I_0(kr_0)} + \frac{\rho_g}{\rho_l} \left(u_{rel} - \frac{i\omega}{k} \right)^2 k^2 \left(\frac{l^2 - k^2}{l^2 + k^2} \right) \frac{I_1(kr_0) K_0(kr_0)}{I_0(kr_0) K_1(kr_0)} \qquad (1)$$

where I_0 and I_1 are modified Bessel functions of the first kind, K_0 and K_1 are modified Bessel functions of the second kind, $k = 2\pi/\lambda$ is the wave number, σ is the surface tension, $l^2 = k^2 + \omega/\nu_l$, ν_l is the kinematic viscosity, ρ is the density, and the prime indicates differentiation. The subscript l stands for liquid while g stands for gas.

The numerical solution of dispersion function shows that there is a single maximum in the wave growth rate curve $\omega = \omega(k)$. It is assumed that the wave with the highest growth rate $\omega = \Omega$ will finally be sheared off the jet and will form new droplets. Curve fits were generated from the numerical solutions to equation (1) for the growth rate of the fastest growing and thus most unstable surface wave,

$$\Omega\left[\frac{\rho_l r_0^3}{\sigma}\right]^{0.5} = \frac{0.34 + 0.38 \cdot We_g^{1.5}}{(1+Z)(1+1.4 \cdot T^{0.6})}, \tag{2}$$

and the corresponding wavelength

$$\frac{\Lambda}{r_0} = 9.02 \frac{(1+0.45 \cdot Z^{0.5})(1+0.4 \cdot T^{0.7})}{(1+0.865 \cdot We_g^{1.67})^{0.6}} \tag{3}$$

where

$$Z = \frac{\sqrt{We_l}}{Re_l}, \quad T = Z\sqrt{We_g}, We_g = \frac{\rho_g r_0 u_{rel}^2}{\sigma}, We_l = \frac{\rho_l r_0 u_{rel}^2}{\sigma}, Re_l = \frac{\rho_l r_0 u_{rel}}{\eta_l}.$$

Z is the Ohnesorge number, T is the Taylor number, *We* is the Webber number, *Re* is the Reynolds number and r_0 is the radius of the undisturbed jet.

Reitz [10] applied this theory to the modelling of the breakup of liquid droplets with radius *r*. Again, waves grow on the drop surface with a growth rate Ω and a wave length Λ. Because the new child drops are formed from the surface waves that are sheared off the parent drops, it is assumed that the size of the new droplets is proportional to the wavelength Λ,

$$r_{new} = B_0 \cdot \Lambda, \tag{4}$$

where $B_0 = 0.61$ is a constant, the value of which is fixed. A new parcel containing product drops of size r_{new} is created and added to the computations. In contrast to the TAB model, the parent drop does not perform a complete breakup, but continuously looses mass while penetrating into the gas. This results in a shrinking radius whose rate of reduction at a certain time depends on the difference between the actual value of droplet radius r and an equilibrium droplet size (which is equal to the child droplet radius r_{new}) as well as on the value of a characteristic time span, τ_{bu}:

$$\frac{dr}{dt} = -\frac{r - r_{new}}{\tau_{bu}}, \tag{5}$$

$$\tau_{bu} = 3.788 \cdot B_1 \frac{r}{\Lambda} \cdot \Omega. \tag{6}$$

B_1 is an adjustable model constant including the influence of the nozzle hole flow (turbulence level) and nozzle design on spray breakup. Values between $B_1 = 1.73$ and $B_1 = 60$ are proposed in the literature. A higher value of B_1 leads to reduced breakup and increased penetration, while a smaller value, on the other hand, results in increased spray disintegration, faster fuel-air mixing, and reduced penetration.

Although stripping breakup is one of the most important breakup mechanisms in the case of high-pressure injection, experiments have shown that the formation of strong bimodal droplet size distributions obtained with the KH model is unrealistic, and that another important mechanism, the sudden disintegration of a complete drop into droplets with diameters much bigger than those of the KH-child droplets is important near the nozzle. For this reason, the KH-model is usually combined with the Rayleigh-Taylor model.

The Rayleigh-Taylor (RT) model is based on the theoretical work of Taylor [3], who investigated the instability of the interface between two fluids of different densities in the case of an acceleration (or deceleration) normal to this interface. Droplet and gas are moving with velocity u_{rel} relative to each other. The deceleration of the drop (in the forward direction) due

to drag forces can be treated as an acceleration of the drop in the direction of the airflow (backward direction). Thus, instable waves can grow on the back side of the drop, Figure 2.

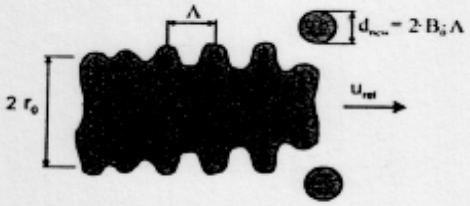

Fig. 1 Scheme of the KH model [3, 10]

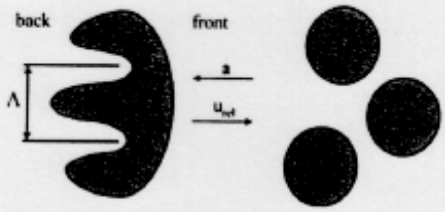

Fig. 2 RT instability on a liquid drop [3]

The disintegration of the drop is induced by the inertia of the liquid if drops and ligaments leaving the nozzle at high velocities are strongly decelerated by the aerodynamic drag force

$$F_{aero} = \pi r^2 c_D \frac{\rho_g u_{rel}^2}{2} \tag{7}$$

Dividing the drag force by the mass of the drop, the acceleration of the interface can be found:

$$a = \frac{3}{8} c_D \frac{\rho_g u_{rel}^2}{\rho_l r}, \tag{8}$$

where c_D is the drag coefficient of the drop. The growth rate and the corresponding wavelength of the fastest growing wave are [3]:

$$\Omega = \sqrt{\frac{2}{3\sqrt{3\sigma}} \frac{\left[a(\rho_l - \rho_g)\right]^{3/2}}{\rho_l + \rho_g}} \tag{9}$$

and

$$\Lambda = C_3 2\pi \sqrt{\frac{3\sigma}{a(\rho_l - \rho_g)}}. \tag{10}$$

The break-up time $t_{bu} = \Omega^{-1}$ is found to be the reciprocal of the frequency of the fastest growing wave. At $t = t_{bu}$ the drop disintegrates completely into small droplets whose radius $d_{new} = \Lambda$ is assumed to be proportional to the wavelength. The drop is only allowed to break up if Λ is smaller than its diameter. The number of new drops is calculated using the mass conservation principle. C_3 is an adjustable constant that includes the unknown effects of the turbulence and cavitation inside the nozzle.

The RT breakup mechanism describes the catastrophic breakup mode which occurs when high relative velocities result in strong deceleration. However, the reduction of droplet size by the RT model is too fast if it is applied to drops just leaving the nozzle hole. Thus, the RT model is applied to the spray breakup only beyond a certain distance from the nozzle. This distance is defined as breakup length L_b of the dense fragmented core (11). Only the KH stripping breakup is allowed to occur near the nozzle, as shown in Figure 3.

$$L_b = C_{BU} \cdot D_{nozzle} \sqrt{\frac{\rho_l}{\rho_g}} \tag{11}$$

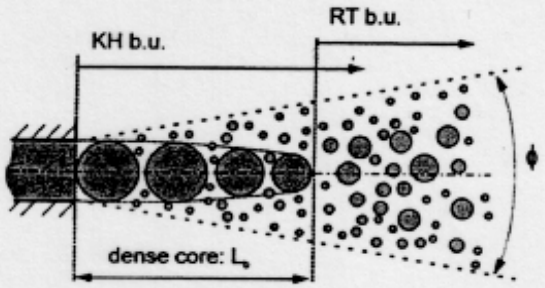

Fig. 3 Combined KH-RT model [3]

3. Variation of Spray Constants

In the first part of the paper, the influence of the KHRT model parameters on the fuel spray was analyzed. In order to perform simulations, a structured mesh of the size of 20 x 20 x 100 mm was built. The mesh consists of 50 x 10 x 10 cells. Since the spray is axis symmetric, only 1/4 of the spray was simulated in order to save computing resources and calculation time. Cell size grading was used on the mesh edges in order to obtain a cell size of 1 mm in the injection region, which is reported by [4] to be a good value for similar calculations.

The initial and boundary conditions were set in order to match those of the experimental case settings, found in [15]. The ambient temperature was set to 1000 K and the pressure to $4.33 \cdot 10^6$ Pa. The fuel physical properties were set to those of normal heptane C_7H_{16}. The injected mass was 0.017 mg while the injection duration was 0.008 s, the same as for the experimental settings. The droplet collision and the combustion models were turned off in order to reduce the number of influential parameters. The RNG k-ε turbulence model was used. The OpenFOAM standard evaporation model was used. A simple blob injection model was used to introduce the droplets into the calculation domain.

The KHRT model implemented in OpenFOAM has several parameters. Some of them, i.e. B0, WebberLimit, msLimit and Ctau, are fixed, while the others are intended to tune in order to match the unknown influence of the nozzle internal flow. In this study, the B1, CBU and C_3 (renamed CRT in the OpenFOAM model) parameters are varied in order to analyze their influence on the spray. The resulting spray was analyzed by considering the following parameters: SMD (Sauter Mean Diameter), liquid length, vapour penetration and evaporated mass. The Sauter mean diameter is the average volume of all the droplets divided by their average surface (12):

$$SMD = \frac{\sum_{i=1}^{N} d_i^3}{\sum_{i=1}^{N} d_i^2} \tag{12}$$

The liquid length is defined as the distance of the limit of 99% of the liquid mass from the nozzle. The vapour penetration is the distance from the nozzle of the limit where the fuel mass fraction in the gas phase is greater than 0. The evaporated mass is the mass of fuel that has been transferred from the liquid to the gas phase. Additionally, a visual comparison of the simulated sprays was done. The comparison gives the size and position of droplets and the fuel mass fraction space distribution for the time of 2 ms after the start of injection.

3.1. Coefficient B1

The B_1 parameter influences directly the breakup time τ_{bu}, as it can be seen from equation (6). This makes the droplets break up later, so the average droplet size increases for bigger B1 values. This can also be concluded after a simulated spray analysis. It can be seen that bigger B1 values result in bigger droplets, Figure 4. For B1=5, the SMD value is about 3.3 μm, for B1=10 SMD, it is about 27.3 μm, while for B1= 15, it is about 47 μm. Bigger droplets have greater mass and it takes longer to heat them. Hence, bigger droplets evaporate more slowly and have greater inertia. These are the reasons why they fly further from the nozzle, which can be seen in the liquid length graph, Figure 5. The liquid phase for B1=5 reaches just about 0.006 m from the nozzle before evaporating completely. For the value of B1=10, it reaches 0.032 m, while for B1=15, it arrives to 0.052 m from the nozzle. Bigger droplets fly faster and further. The same mechanism allows a slightly faster vapour penetration with greater B1 values since bigger droplets transfer the fuel mass further from the nozzle and the evaporation process goes on at that more distant location. In Figure 6, one can see that the fuel vapour for greater B1 values penetrates into the chamber faster, especially in the first part of the injection process. Higher inertia allows bigger droplets to fly further and evaporate there, while drag has a greater influence on smaller droplets which evaporate closer to the nozzle. In the second part of the process, the air is accelerated by the spray, the velocity difference between the liquid and the gas phase is reduced and hence drag is reduced. This is the reason why the vapour penetration difference is smaller in the second part of the injection process. In the evaporated mass diagram, Figure 7, one can see that the evaporation is slower for bigger B1. Evaporation is a process that takes place on the droplet surface and smaller drops have a bigger surface-to-mass ratio. Another reason for the faster evaporation of the smaller drops is that their smaller mass gets heated in a shorter time.

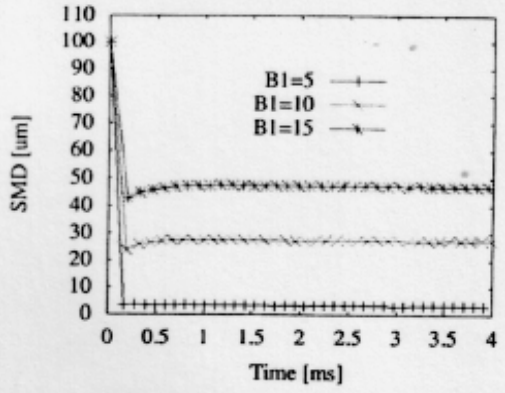

Fig. 4 The SMD for different B1

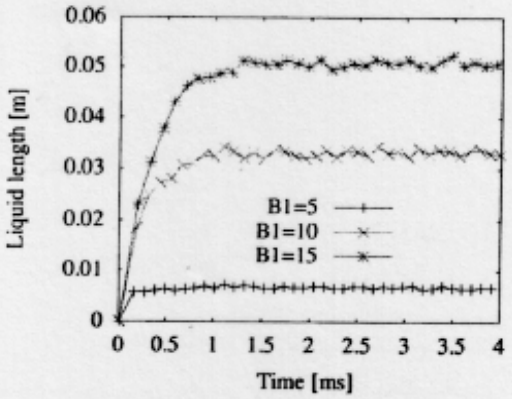

Fig. 5 The liquid length for different B1

The strong influence of B1 can be best seen from the spray result visualization, Figure 8. The droplet size is much smaller for B1=5 than for other cases. The bigger droplets penetrate into the middle of the domain for the case with B1=15. Generally, the highest fuel vapour concentration is found in the region just downstream from the last droplets, where the total amount of liquid phase evaporates to the gas phase. The consequence of different droplet size and penetration is a different fuel vapour concentration distribution. For B1=5 and small droplets there is a very high fuel vapour concentration (0.4 kg of fuel per kg of mixture) in the region just downstream from the nozzle. The high fuel mass fraction is a result of the fast evaporation of small droplets. The location close to the nozzle is a result of the small liquid penetration due to the small droplet inertia. For bigger values of B1, bigger droplets result in the greater liquid phase penetration and slower evaporation. Hence, the highest fuel mass fraction region is translated downstream and the highest fuel mass fraction is lower (0.29 for

B1=10 and 0.26 for B1=15). In Figure 8 one can also notice that the tip of the spray (the fuel vapour) is more spread for the sprays with higher B1 values and it gets a characteristic mushroom shape.

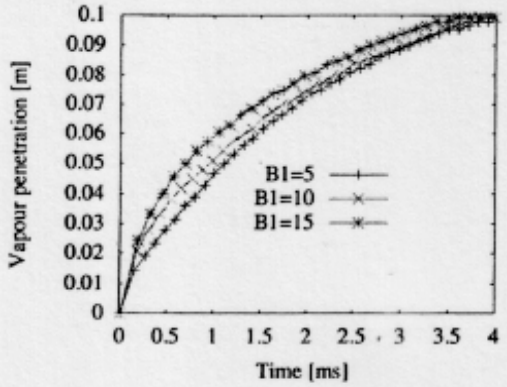

Fig. 6 The vapour penetration for different B1

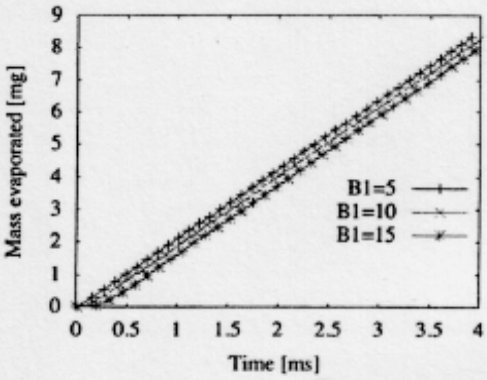

Fig. 7 The evaporated mass for different B1

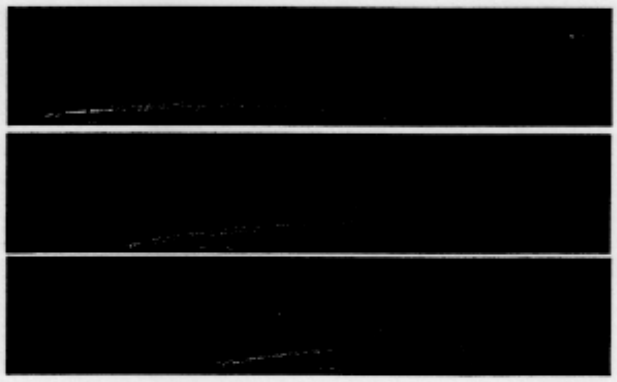

Fig. 8 The spray visualization comparison at 2 ms for different B1 values

3.2. Coefficient CBU

The CBU coefficient from equation (11) regulates the spray core length by blocking the RT (catastrophic) breakup to a certain distance from the nozzle. From Figure 9 one can see that by increasing the CBU value, a smaller average droplet size is produced. For CBU=5, the SMD value is around 60 μm, for CBU=10, it is around 45 μm, while for CBU=20, it is around 20 μm. As a consequence, for smaller CBU values, bigger droplets penetrate further into the gas phase, Figure 10. The liquid length is 0.06 m for CBU=5, 0.05 m for CBU=10, and it oscillates around 0.025 m for the value of CBU set to 20. The vapour penetration also reflects the influence of the droplet size, Figure 11. The fuel vapour penetrates into the domain fastest for the value of CBU=5, while it is slowest for the value of CBU=20, especially in the first part of the injection process. Another consequence of the different average droplet size is the evaporation intensity. Figure 12 shows that the fastest to evaporate are the droplets for the value of CBU set to 20. The evaporation for CBU=10 is slightly slower while for CBU=5, it is the slowest of the tested cases.

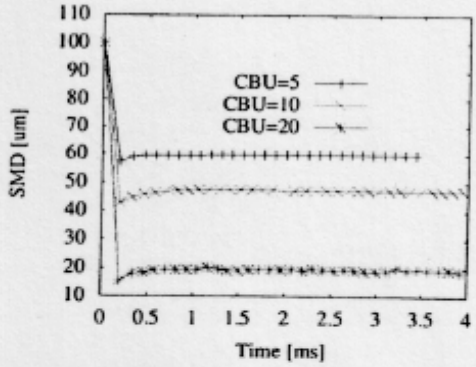

Fig. 9 The SMD for different CBU

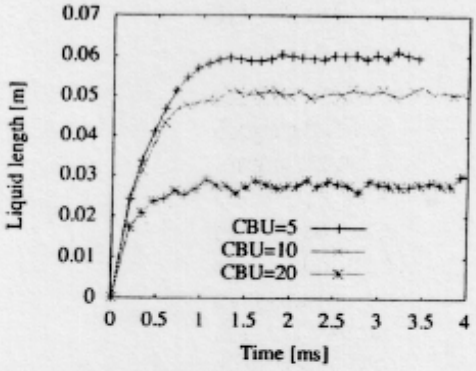

Fig. 10 The liquid length for different CBU

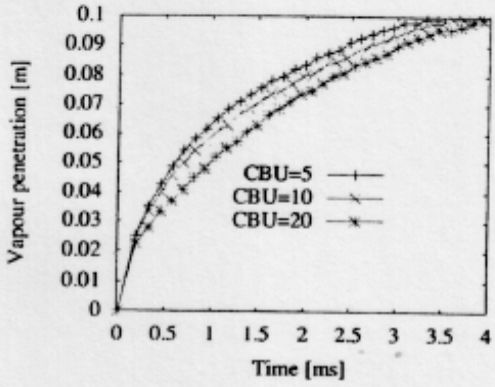

Fig. 11 The vapour penetration for different CBU

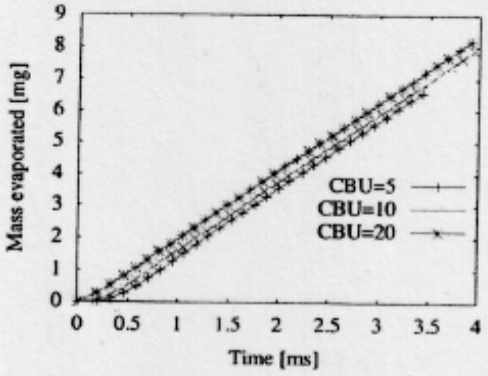

Fig. 12 The evaporated mass for different CBU

The simulation results are visually presented in Figure 13. The first thing that can be noticed is the droplet size and penetration that decrease for increasing CBU values. For CBU=5, the droplets are bigger and reach almost 2/3 of the domain. For the other cases, CBU=10 and CBU=20, the droplets are smaller and they disappear earlier due to evaporation. Since bigger droplets fly further, they transfer the fuel mass further and evaporate in a farther location. Hence, the fuel vapour cloud is longer for smaller values of CBU. As far as fuel mass fractions in the gas phase are concerned, smaller droplets evaporate faster. As a consequence, fuel mass fraction levels are higher for bigger values of CBU.

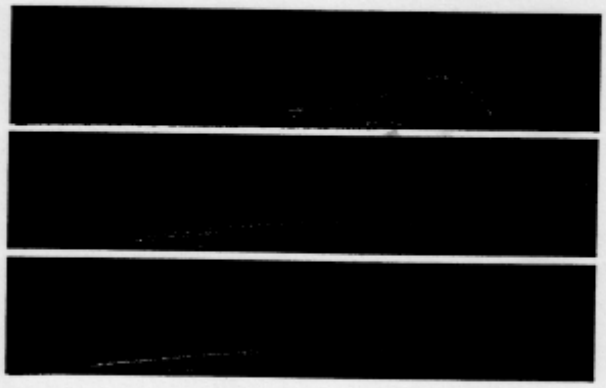

Fig. 13 The spray visualization comparison at 2 ms for different CBU values

3.3. Coefficient CRT

The CRT coefficient from OpenFOAM is equivalent to the C_3 constant from the mathematical model (10). It is used to regulate the wave length and the size of newly created drops after the RT breakup. Accordingly, for grater values, bigger drops are generated and a longer liquid length is obtained. In Figure 14 it can be seen that the SMD is around 50 μm for CRT=5, it is 45 μm for CRT=2, and 37 μm for CRT=1. Since bigger droplets fly further, as explained earlier in the text, it follows that the liquid length varies from 0.04 m for CRT=1 to over 0.05 m for CRT=5, Figure 15. The influence on the vapour penetration and on the evaporation rate is limited for the tested range of the CRT value. But still, it can be noticed that the vapour penetration is slightly faster for bigger CRT, Figure 16, and that evaporation is a bit faster for smaller values of the CRT coefficient, Figure 17.

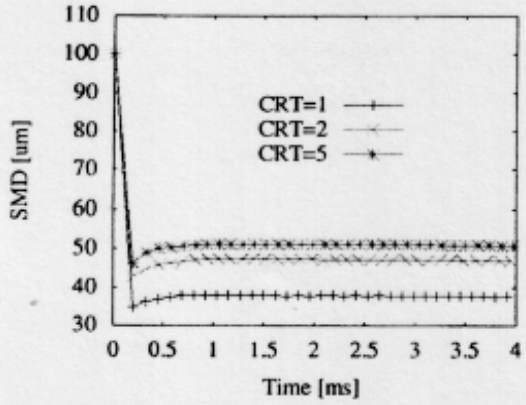

Fig. 14 The SMD for different CRT

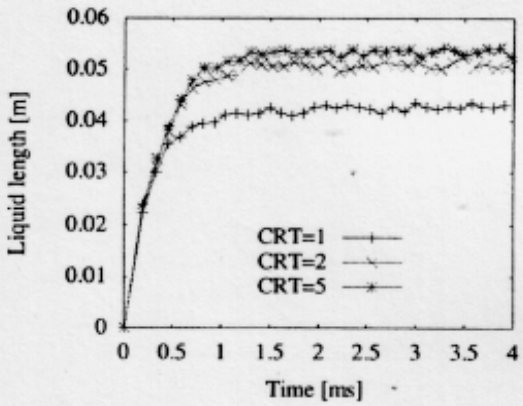

Fig. 15 The liquid length for different CRT

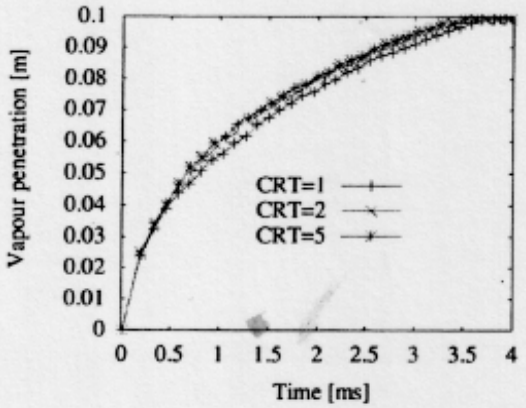

Fig. 16 The vapour penetration for different CRT

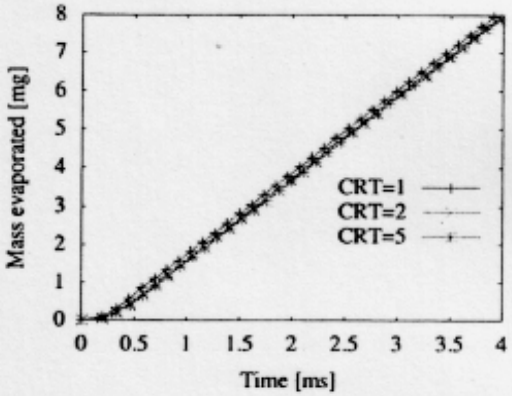

Fig. 17 The evaporated mass for different CRT

The small influence for the tested range of CRT values is also shown by the visual presentation of the spray for the time of 2 ms, Figure 18. However, it can be noticed that for smaller values of CRT the liquid core is shorter, droplets are smaller and the fuel vapour mass fractions are higher.

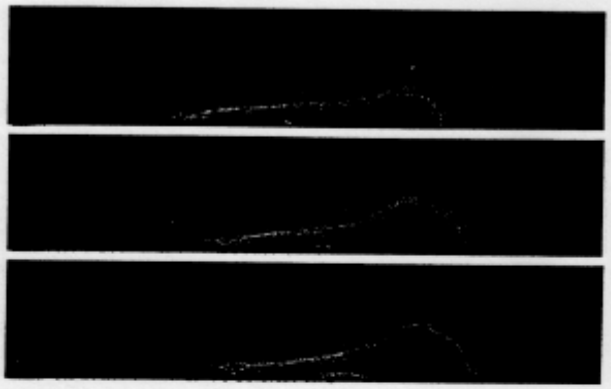

Fig. 18 The spray visualization comparison at 2 ms for different CRT values

4. Selection of the spray model parameters

According to the experience gained in the previous analysis, a set of spray model parameters was chosen in order to reproduce the experimental results reported by [15] for the same nozzle geometry, fuel (n-heptane), injection parameters and ambient conditions. A blob injector model was used in combination with a blob KHRT atomization model, with the settings reported in Table 1.

Table 1 OpenFOAM KHRT atomization model parameters

Parameter	Value
B0	0.61
B1	8.0
WeberLimit	6
msLimit	0.02
CBU	8.0
Ctau	1

Figure 19 shows an excellent vapour penetration matching. The experimental liquid length is 9.2 mm, while the simulated liquid penetration is about 30 mm. The difference seems to be very big. However, these values are not comparable since they are obtained in a different manner. The experimental result was obtained by introducing a 532-nm, continuous-wave laser beam to flood illuminate the spray, while an image of the Mie-scattered light was acquired with an intensified camera orthogonal to the spray. A narrow band-pass filter at the laser wavelength (532 nm) was used to minimize the collection of other emission sources, such as combustion luminosity. The analysis of the Mie-scattered light images for the liquid length involved determining the maximum axial distance in the spray where the light intensity was above a threshold equal to 3% of the light intensity range measurable with the camera. This definition of liquid length was found to be relatively insensitive to big changes in parameters such as the laser power and the camera gain due to the rapid decline in the scattered light intensity at the leading edge of the liquid region [15]. The simulated measure is obtained by calculating the distance of the limit of 99 % of the liquid mass from the nozzle. The first consideration is that it is hard to define and distinguish the border where the spray consists of liquid droplets of infinitesimal size or of dense vapour region. In the simulation, there is no 'liquid core' since larger, but spherical and discrete droplets are injected directly from the nozzle. For these reasons, experimental liquid length is not usable as an absolute value but only for a comparison of trends.

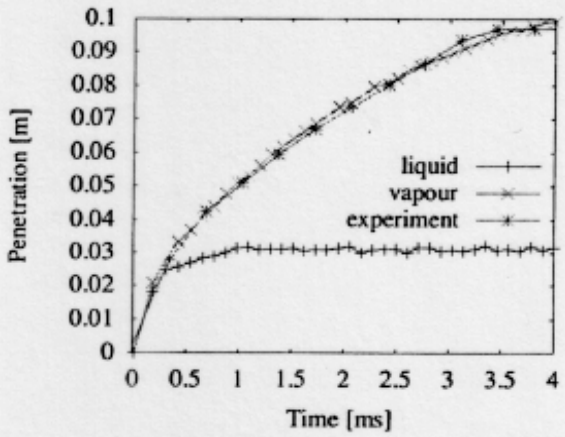

Fig. 19 The simulated liquid and vapour penetrations compared to the experimental penetration

A visual comparison between the experimental results (lower part) and simulation results (upper part) is given for the times of 0.7, 1.4, 2.1, and 2.8 ms in Figure 20. This kind of comparison is useful because the region involved in the process of mixture formation can be observed, which is essential for obtaining the local equivalence ratio. The experimental results are obtained by shadowgraph imaging technique. The shadowgraph imaging was performed by collimating broadband emission from a xenon arc lamp, passing the light through a line-of-sight in the combustion vessel, and then using a concave mirror to direct the light directly onto the camera sensor. Shadowgraph imaging, like Schlieren imaging, is sensitive to gradients in refractive index, formed by either density or composition differences along the line-of-sight. Applied to vaporizing diesel sprays, shadowgraph imaging identifies the vapour boundary of the penetrating jet [15]. In the simulation results, several transparent isosurfaces presenting constant mass fractions are displayed.

Very good matching is found between the simulation and the experiment, especially for the vapour tip penetration. The fuel vapour region obtained by simulation is a bit wider than the experimental one, especially in the initial phase around 0.7 ms.

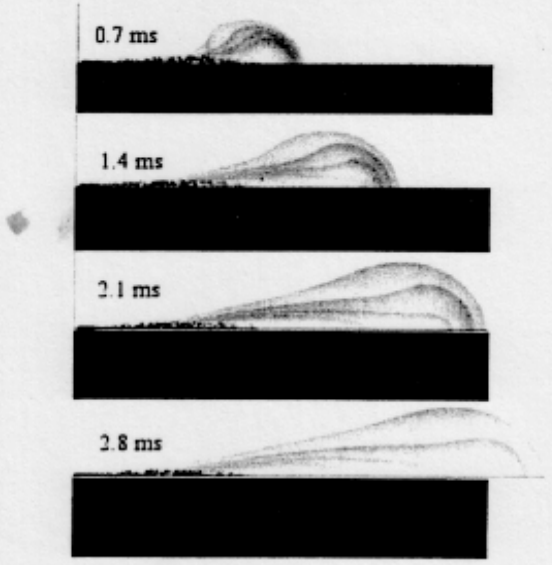

Fig 20 A visual comparison of the simulated spray presented with isosurfaces and droplets with the experimentally obtained pictures of the spray for the times of 0.7, 1.4, 2.1 and 2.8 ms.

5. Conclusions

In the first part of the article, the KHRT spray model was evaluated. The influence of the spray model parameters B1, CBU, and CRT was analyzed. The SMD analysis showed that the mentioned model parameters influence the droplet size directly or indirectly, by influencing the breakup time. It was concluded that an increasing B1 increases the resulting droplet size, an increasing CBU decreases the droplet size, and an increasing CRT increases the droplet size. A direct consequence of bigger droplet size is its higher inertia and slower evaporation. For this reasons, sprays with bigger droplets have grater liquid lengths and faster fuel vapour penetration. From the visualized spray results it can be concluded that the high fuel mass fraction region is located further downstream for bigger droplets than for smaller ones. Higher fuel mass fractions are reached for smaller droplets than for bigger droplets. After the analysis of the influence of spray model parameters, a set of parameters was chosen in order to reproduce the experimental results of n-heptane injection in the Sandia combustion chamber. The experimental fuel vapour penetration and distribution matched very well. On the other hand, it was concluded that the experimental and simulation liquid lengths were not comparable since they were obtained in different manners.

REFERENCES

[1] Amsden, A.A., O'Rourke, P.J., Butler, T. D.: KIVA-II – A Computer Program for Chemically Reactive Flows with Sprays. Los Alamos National Laboratories, LA-11560-MS, 1989

[2] Amsden, A.A., Ramshaw, J.D., O'Rourke, P.J., Dukowicz, J.K.: KIVA.. A Computer Program for Two- and Three-Dimensional Fluid Flows with Chemical Reactions and Fuel Sprays. Los Alamos National Labs, Rept LA-10245-MS, 1985

[3] Baumgarten, C.: Mixture Formation in Internal Combustion Engines, Springer-Verlag Berlin Heidelberg 2006

[4] D'Errico, G., Ettorre, D., Lucchini, T.: Simplified and Detailed Chemistry Modeling of Constant-Volume Diesel Combustion Experiments , SAE paper 2008-01-0954, 2008

[5] Heywood, J.B.: Internal Combustion Engine Fundamentals. McGraw-Hill, New York, 1988

[6] Hiroyasu, H., Arai, M.: Structures of Fuel Sprays in Diesel Engines. SAE-paper 900475, 1990

[7] Hiroyasu, H., Kadota, T.: Fuel Droplet Size Distribution in Diesel Combustion Chamber, SAE paper 740715, 1974

[8] Kralj, Č.: Numerical simulation of diesel spray process, PhD dissertation, Imperial College, London, 1995

[9] Park, S.W., Kim, H. J., Lee, C. S.: Investigation of Atomization Characteristics and Prediction Accuracy of Hybrid Models for High-Speed Diesel Fuel Sprays. SAE paper 2003-01-1045, 2003

[10] Reitz, R. D.: Modeling Atomization Processes in High-Pressure Vaporizing Sprays. Atomization and Spray Technology 3, pp 309–337 , 1987

[11] Reitz, R. D., Bracco, F.B.: On the Dependence of Spray Angle and Other Spray Parameters on Nozzle Design and Operating Conditions, SAE paper 790494, 1979

[12] O'Rourke, P. J., Amsden, A. A.: The Tab Method for Numerical Calculation of Spray Droplet Breakup, SAE paper 872089, 1987

[13] Versteeg, H. K., Malalasekera, W.: *An introduction to computational fluid dynamics - The finite volume method*, Longman Scientific & Technical, England, 1995.

[14] *OpenFOAM: The Open Source CFD Toolbox, http://www.openfoam.com/*

[15] Engine Combustion Network, Sandia National Laboratories, https://share.sandia.gov/ecn/

Submitted: 03.12.2010

Accepted: 05.01.2011

Tomislav Senčić[1]
Tommaso Lucchini[2]
Vedran Mrzljak[1]
1 Faculty of Engineering, University of Rijeka, Vukovarska 58, 51000 Rijeka, Croatia
2 Politecnico di Milano, via Lambruschini 4, I-20156 Milano, Italy